Scientia Iranica B (2014) 21(2), 438–448

Sharif University of Technology
Scientia Iranica
Transactions B: Mechanical Engineering
www.scientiairanica.com

Investigation into the effect of intake port geometric parameters and blockage on flow coefficient and in-cylinder flow: Application to engine port design

A. Mohammadebrahim[a,b], S. Kazemzadeh Hannani[a,*] and B. Shafii[a]

a. *School of Mechanical Engineering, Sharif University of Technology, Tehran, P.O. Box 11155-9567, Iran.*
b. *Irankhodro Powertrain Co. (IPCO), Tehran, P.O. Box 13445-1497, Iran.*

Received 27 November 2012; received in revised form 11 August 2013; accepted 21 September 2013

KEYWORDS
Internal combustion engine;
Inlet port;
Flowbench;
Steady flow test;
Flow coefficient;
Swirl;
Tumble;
CFD.

Abstract. The Computational Fluid Dynamics (CFD) method is employed to gain further insight into the characteristics of the in-cylinder flow field. Comparison between the measured and predicted results of the in-cylinder tumble flow and flow coefficient generated by a port-valve-liner assembly, on a steady-flow test bench, is presented, and a reasonably good level of agreement is achieved. A CAD parametric model of port geometry is created to enable variations, practically and quickly. Employing CFD analysis, the relationship between design parameters and port flow characteristics is established. The influence of new blockage patterns on in-cylinder flow is also studied.

1. Introduction

The design of inlet ports for spark ignition internal combustion engines has a direct and well-known influence on their performance and emissions as a result of changes in volumetric efficiency and fuel burn rate [1]. The design of ports is becoming more critical as SI engines are developed further to meet increasingly stringent exhaust emission legislations. Lately, further emphasis has been placed on port design by the re-emergence of the direct injection gasoline engine. Inlet port design is additionally influenced by external factors, such as packaging, valve and valve train design, capacity and application [2].

Improvements in computer processing power and fluid simulation codes have resulted in rapid advancements in computer-based engine simulation. The use of three-dimensional CFD codes allows for better understanding of flow dynamics in parts of a gas exchange system, before any prototypes are ever manufactured [3].

In fact, many manufacturers are routinely utilizing CFD as part of their engine design process [4,5]. Steady-state CFD simulation comparison with steady-state flow bench results has been widely applied in academic and industrial research. Many researchers have focused on the improvements of volumetric efficiency, tumble ratio, and swirl ratio [6] (Figure 1). Guy et al. [7] used the commercial CFD package, Fluent, to complement the traditional optimization strategies. They studied the flow coefficient of a racing car using both CFD simulation and experiment. A comparison of results between a CFD prediction and a flow bench measurement demonstrated the validity and usefulness of this approach.

Extensive investigations have been reported on

*. *Corresponding author. Tel.: +98 21 66165508; Fax: +98 21 66000021*
E-mail addresses: m_ebrahim@mech.sharif.edu (A. Mohammadebrahim); hannani@sharif.edu (S. Kazemzadeh Hannani); behshad@sharif.edu (B. Shafii)

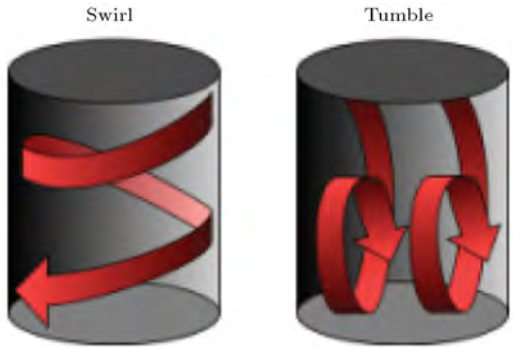

Figure 1. Swirl and tumble in the engine cylinder.

the subject of validation of the CFD codes with the flow field measurements of internal combustion engines [8] and, while experimental techniques can render acceptable parameter sensitivity results [9-11], such an approach is exhaustive, expensive and time consuming. Both experimental and numerical methods still have a long way to go to be improved from an academic and industrial viewpoint. Nevertheless, for industrial applications, they are useful design tools, provided that the errors are within acceptable limits. Ongoing progress for the development of CAE tools has led to the creation of new methodologies. CFD calculations provide insight into the details of port and in-cylinder flow, thus, enabling efficient optimization.

In addition to the intake port geometry design, another method of generating different charge motion characteristics is to place flow blockages or vanes in the intake duct. Selamet et al. [12] reported the impact of different intake runner blockages, which created different kinds of tumble and swirl intensity in an SI engine, on combustion characteristics and engine-out emissions.

The flow bench test of a cylinder head is particularly useful for evaluating the static flow coefficient and making compromises to trade off between the engine flow capacity and the swirl or tumble strength. This test is a widely adopted procedure in the development of engines. It is used to assist and assess the design of the engine ports and the combustion chamber concerning engine flow capacity and the in-cylinder flow pattern of the charge motion, which are critical to the engine combustion performance. The flow bench test is also an important source of input data for the engine simulation code, which usually requires the non-dimensional and normalized intake flow parameters across the range of valve lifts. The correlation between the static flow coefficient and engine breathing capacity is simpler, but that between the swirl/tumble ratio and the combustion performance is not straightforward. There is much research that presents the correlation between in-cylinder flow (swirl and tumble) and combustion performance, such as heat release ratio, flame structure, equivalence ratio, pressure rise ratio, and

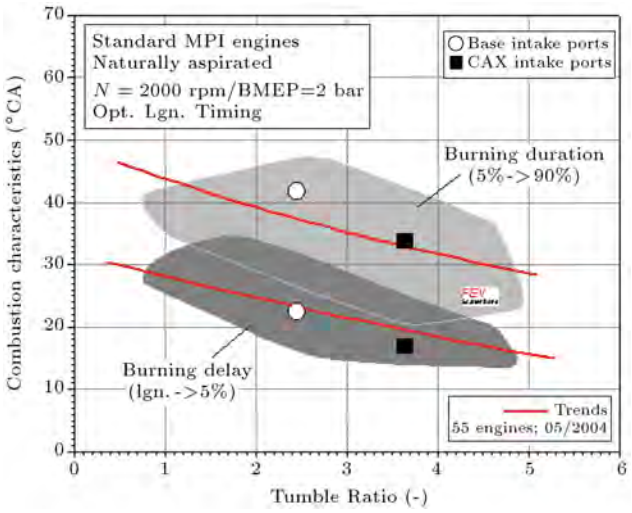

Figure 2. Effect of charge motion intensity on combustion characteristics [15].

combustion duration, etc. [13,14]. Adomeit at FEV [15] proposed a correlation between the tumble ratio and combustion characteristics based on the test results of fifty different MPI, naturally aspirated, SI engines (Figure 2).

In the present study, after comparison between the measured and predicted results of in-cylinder flow, CFD analysis is employed to establish the relationship between design parameters and port flow characteristics. Firstly, different turbulence models are applied and compared, and swirl/tumble are calculated and presented in some planes. The results are useful to study the decay of swirl/tumble magnitudes from the top to the piston surface. With parametric study, new intake ports can be designed based on desirable flow parameters. Also, innovative patterns of intake runner blockages are studied to produce various kinds of charge motion. This study will be applicable to engine port design. In some design applications, high tumble or swirl intensity is desirable. In some others, volumetric efficiency is important and sometimes trade-off between design parameters is expected.

2. Experimental test

The experimental set up is shown in Figure 3 schematically. Special mechanisms and fixtures are used to set valve lifts by the clock. In standard tests on engines with four valves per cylinder, inlet or outlet valves are opened simultaneously. A test is performed on the cylinder head and a dummy cylinder is used with a diameter equal to the engine bore. Pressure drop is measured with a stagnation pressure gauge relative to atmospheric pressure. A manometer is used to determine the pressure drop in the orifice and, consequently, to measure volume flow rate. Desired differential pressures are supplied with a bypass valve

(10), and air flow temperature is measured using a temperature gauge for air mass flow rate correction. A swirl meter measures tumble and/or swirl intensity, based on its orientation.

The fan (13) is used to suck air from ambient to simulate an actual state in the engine. If a swirl meter is placed at the orientation shown in Figure 3, with the adaptor and the air box, it will measure tumble intensity. But, if it is placed under a dummy cylinder (Figure 4), it can measure swirl intensity.

Generally, a swirl meter measures the rotational speed of a paddle wheel (because of inlet air flow) as the intensity of swirl or tumble (Figure 4(a)), or, as shown in (Figure 4(b)), a torque can be applied from the air to a honeycomb to take into account the intensity of the swirl or tumble. In our research, a honeycomb type is used and an adaptor is used to measure tumble. All dimensions in Figure 4 are standardized, based on the engine geometry.

The standard test for the inlet port consists of measuring the flow coefficient, swirl and tumble intensities for different valve lift. In this test, after applying the desired differential pressure, the valve lift is set at a certain level (Figure 5).

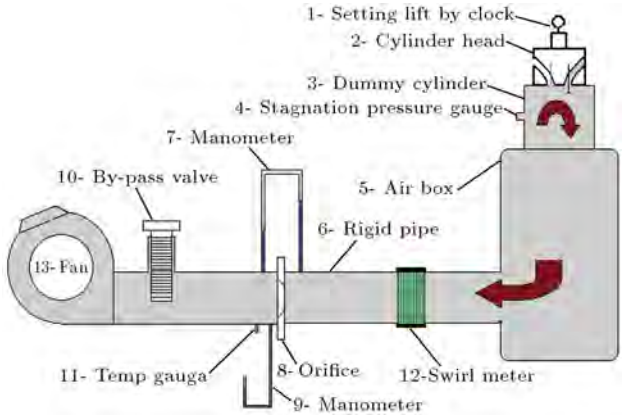

Figure 3. Schematic diagram of the experimental setup.

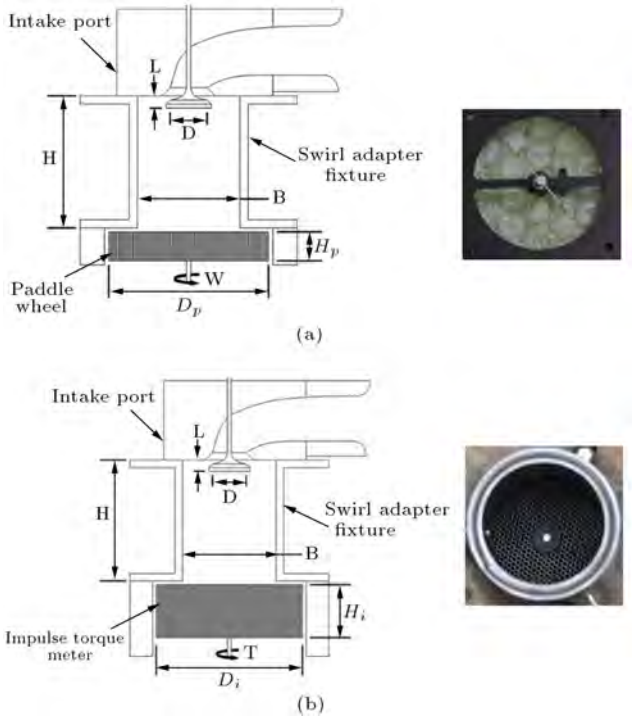

Figure 4. Swirl meter types: (a) Rotational speed measurement; and (b) torque measurement [16].

3. Computer simulation and comparison with experimental results

Computer simulations of the steady flow test for the same engine (Table 1) are conducted on a workstation using Fluent.

Because of the symmetry in the cylinder head, a

Figure 5. Valve lift adjustment by the relevant fixtures and dial indicator in the flowbench.

Table 1. Engine specifications.

	EF7-NA engine	
	Bore (mm)	78.6
	Stroke (mm)	85
	Displacement (cc)	1650
	Inlet port diameter (mm)	**27**
Inlet Valve	Diameter (mm)	30.6
	Stem diameter (mm)	6
	maximum lift (mm)	10
	Seat angle (deg)	44.5
	Inclination (deg)	26

Table 2. Problem set-up.

Function	Setting
Solver	Steady
Temporal discretization	Implicit
Pressure discretization	2nd order upwind
Momentum discretization	2nd order upwind
Pressure-velocity coupling	PISO
Energy discretization	2nd order upwind
Turbulence modeling	RNG $k-\varepsilon$
Near wall treatment	Standard wall function
Fluid model	Air (ideal gas)

half model is used. The parameters used in the problem set-up are listed in Table 2.

The boundary conditions for the model are selected to mimic the conditions of the steady-state flowbench. That is, the pressure gradient across the intake and outlet of the system is specified. The inlet flow into the mesh is confined to be normal to the boundary. The results shown in this paper are obtained for a pressure drop of 5.0 kPa, which is commonly used for flowbench testing of conventional engines.

Several tetrahedral meshes of varying resolutions are employed to establish the mesh-independency of the solutions. Starting with the coarsest grid that could be meshed successfully and examining progressively finer grids, the predicted C_f for a valve lift of 8 mm is compared. It is shown in Figure 6 that 99500 tetrahedral cells produce very similar results compared to finer grids.

Reshaping of the grid structure near the interface between the valve seat and the dome cylinder head is performed. Figure 7 shows the final product of the grid generation of the port-valve-liner-adaptor assembly with the dome cylinder head. The grid is denser in the top region, because the flow is expected to be more complicated in this area.

In CFD calculations, seven different turbulence models have been applied, including the RSM model.

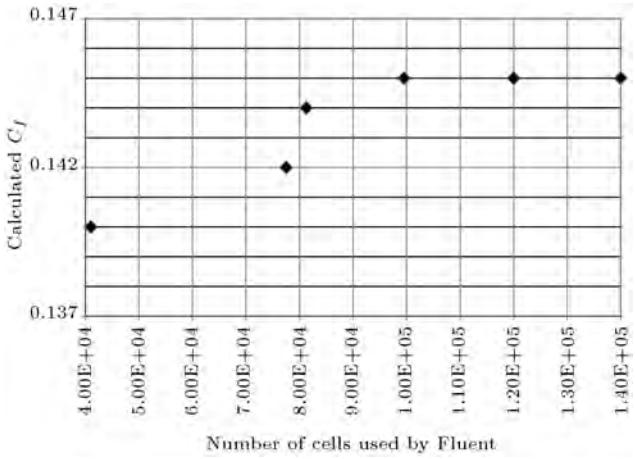

Figure 6. Calculated C_f at lift of 8 mm for various meshing grid sizes.

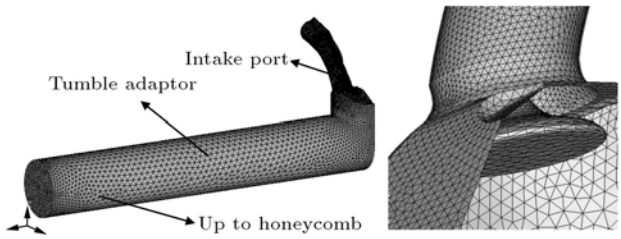

Figure 7. Computational grids of the port-valve-liner assembly with dome-shaped combustion chamber and intake valve seats.

As shown in Figure 8, average vorticity magnitude in the cylinder and mass flow rate at the outlet are independent of the model. These parameters are normalized with maximum values. Maximum difference is 1% in mass flow rate and 9% in vorticity. Also, for more exploration, 10 planes, with 10 mm distance, are defined (Figure 9), and swirl/tumble torques are calculated and compared versus different turbulence models (Figure 10). In summary, based on the computational results, this problem is independent of the turbulence model employed. Finally, the RNG $k-\varepsilon$ turbulence model which performed more robustly for this problem is used with default wall functions. The steady inflow and outflow rates need at least 15000 computational cycles to converge.

A comparison of C_f predicted with the CFD model to the C_f measured on a flowbench is shown in Figure 11. In the case of the low valve lift region, the value of the flow coefficient linearly increases with the

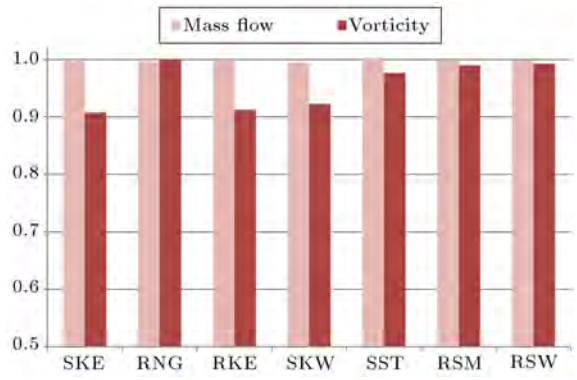

Figure 8. Comparison of mass flow and vorticity for different turbulence models.

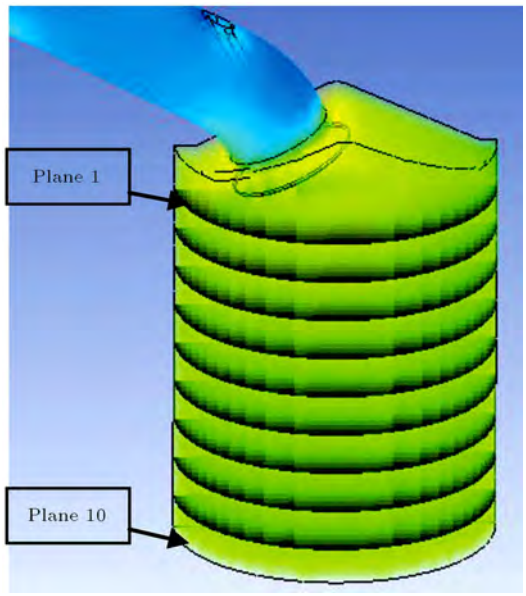

Figure 9. Ten planes with 10 mm distance for swirl/tumble torque calculation.

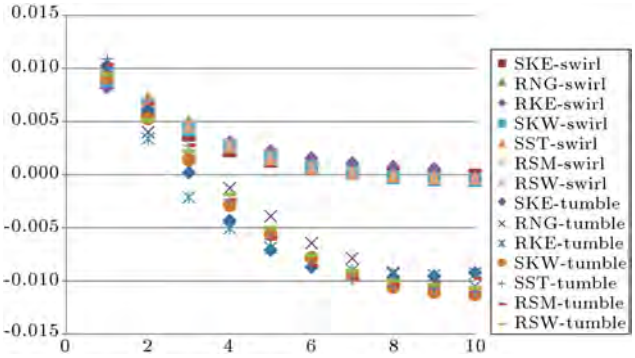

Figure 10. Comparison of swirl/tumble torque (N.m) versus plane number for different turbulence models.

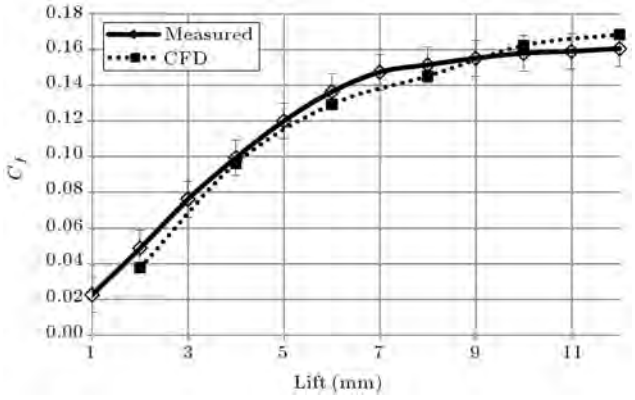

Figure 11. Calculated and measured flow coefficient.

valve lift. On the other hand, in the case of a high valve lift region, the flow coefficient converges to the specific value based on port design and will be independent of valve lift.

The predicted and measured C_f trends are quite similar, which provides more confidence in that the CFD model is able to replicate the main flow trends within the intake system.

A benefit of using CFD to analyze the intake flow is that it is now possible to examine the detailed behavior of the intake flow at any location within the port, head, or cylinder.

The simulation results are illustrated by velocity vector diagrams, as displayed in Figures 12 and 13. Figure 12 reveals that there are two tumble jets inside the cylinder: One is the main jet with a large vortex guided by the dome chamber; the other is a counter rotating jet in a much smaller scale. The maximum velocity is located around the inlet valve curtain. Note that the vectors point downwards at the BDC, because the piston was replaced by the outflow boundary.

Figure 13 shows the velocity vector diagram in three horizontal planes. They are located at 10 mm, 20 mm and 30 mm beneath the TDC. With different scales, the flow patterns show similarities in different

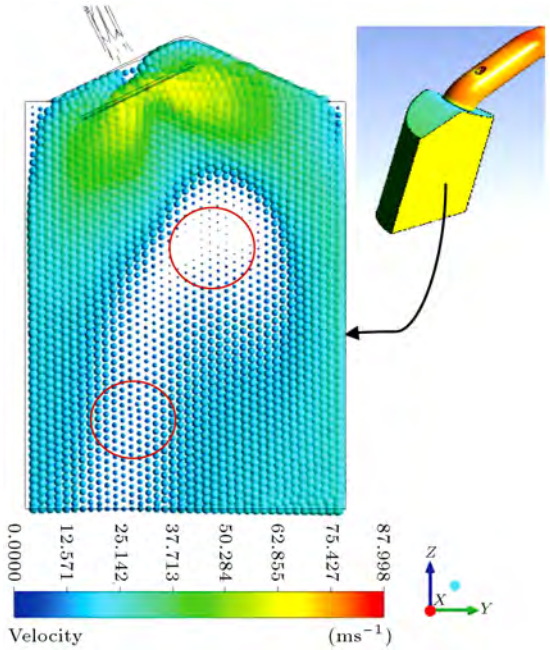

Figure 12. Computed velocity vector diagrams in the YZ plane.

locations. The flow field tends to be more homogeneous as the flow moves further downwards.

The tumble torque is shown in Figure 14. In the case of the low valve lift region, the tumble torque is near zero. On the other hand, in the case of a high valve lift region, the tumble torque linearly increases with the valve lift. As valve lift increases, two small size vortices change to one big size vortex, which is almost the same size as the cylinder bore. In addition, the flow patterns obtained by calculation showed a similar trend to those of the experimental results with a maximum discrepancy of 8%.

4. Parametric study

An idealized inlet port model was created using the Pro/ENGINEER (ProE) CAD package and the following three variables are chosen for parametric study (Figure 15):

- L: Straight height;
- $R1$: Radius of curvature, radius of the centre line of the curve joining the parallel pipe upstream and the valve seat centre line;
- Θ: Port angle, angle between the valve centre line and the centre line of the upstream pipe.

All CFD results are derived at a lift of 7 mm. A 3D tetrahedral mesh of the CAD models, with mesh refinement in areas of large flow parameter gradients, was generated to enable CFD testing. The existence of a symmetry plane allowed only half of the port and cylinder to be modeled.

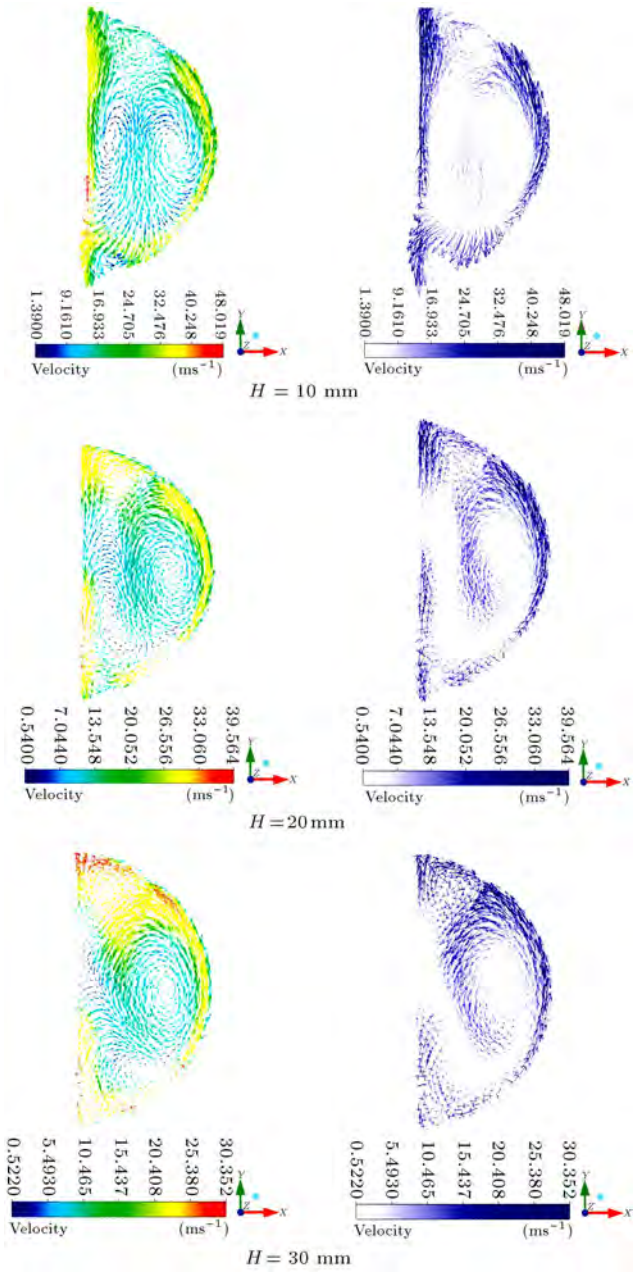

Figure 13. Computed velocity vector diagrams in XY planes, which are located at 10 mm, 20 mm and 30 mm beneath TDC, respectively.

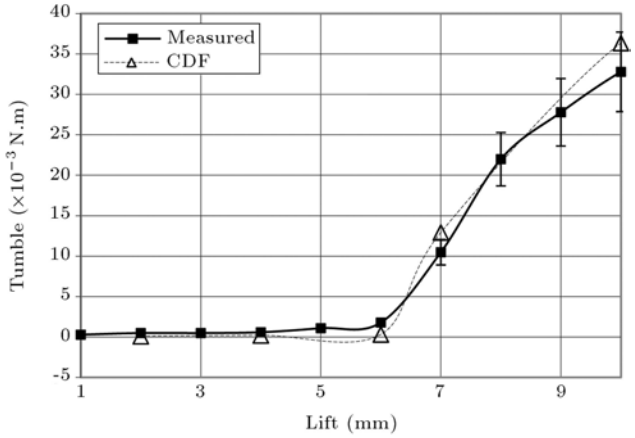

Figure 14. Comparison of simulation and experimental tumble.

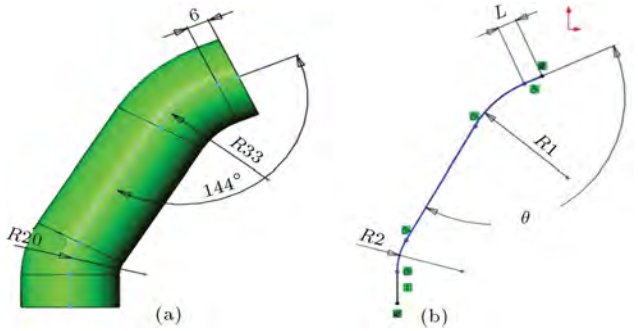

Figure 15. (a) Reference value. (b) Parameterized intake.

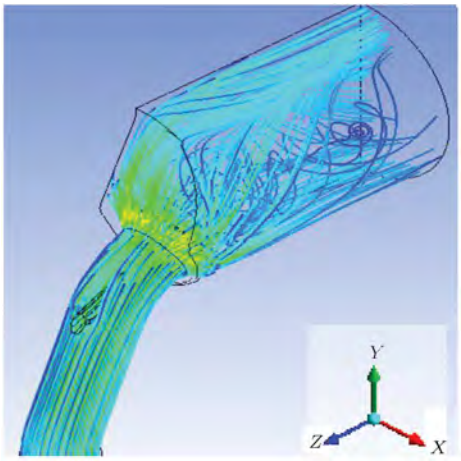

Figure 16. Coordinate axes.

In each section, just one parameter was varied. The aim was sensitivity analyses of each geometric parameter that can be used in new designs.

4.1. Straight height

The base value of L is 6 mm and for the analysis of straight height influence; L is given as 3 mm, 10 mm, 20 mm and 30 mm during the simulation. The torque acting around any axis is calculated based on Figure 16. As shown in Figure 17, when straight height increases, the tumbles torque decreases.

The sensitivity is decreased with increasing straight height, and the decrease is obvious until a height of 10 mm. After that, the steepness of the diagram is smooth. When straight height is 2 times the reference length, tumble torque decreases about 10%. Tumble increases 23% with L equal to 3 mm and reduces 23% while L is 10 mm. Maximum tumble is obtained with L equal to 3 mm. The results indicate that the variation of the straight height had virtually no effect on the swirl and the mass flow rate.

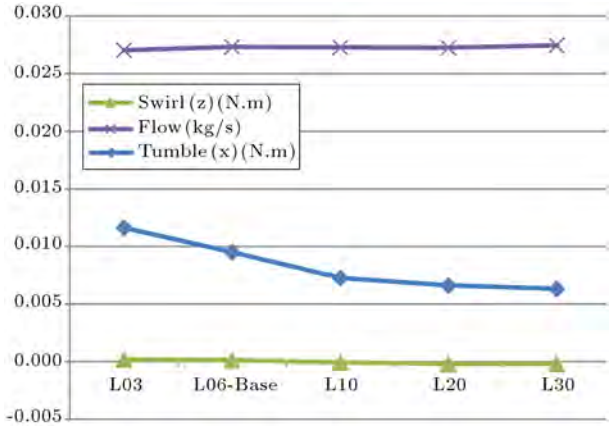

Figure 17. The effect of straight height on flow parameters.

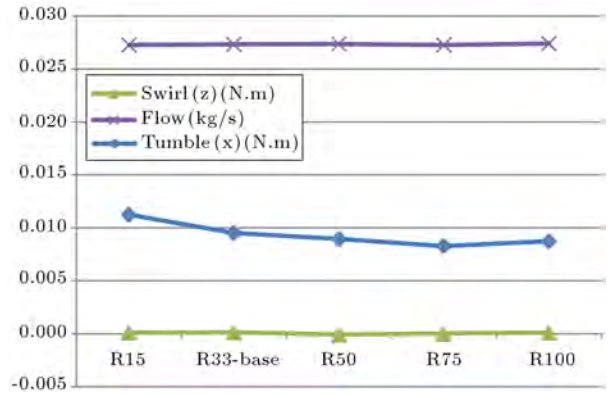

Figure 18. The effect of radius of curvature on flow parameters.

4.2. Radius of curvature

The effect of radius of curvature (R) is shown in Figure 18. R is assigned as 15 mm, 50 mm, 75 mm and 100 mm during the simulation. The base value of R is 33 mm.

As the radius of curvature increases, the tumble torque decreases and, after $R = 75$ mm, the rate of increase is in the order of magnitude of simulation precision. Therefore, the sensitivity of this parameter is decreased and it can be ignored. Tumble increases 22% with R equal to 15 mm and reduces 6% while R is 50 mm. Maximum tumble is obtained with R equal to 15 mm.

Also, the results indicate that the variation of this variable has no significant effect on the swirl intensity and the mass flow rate.

4.3. Port angle

Port angle θ is prescribed as 139°, 144°, 155° and 167°. The base angle value is 144°. As shown in Figure 19, with increasing or decreasing θ, tumbles of the modified models are less than the original. While θ is, respectively 139° or 155°, tumble intensity reduction is 17% and 10%, respectively. Therefore, the

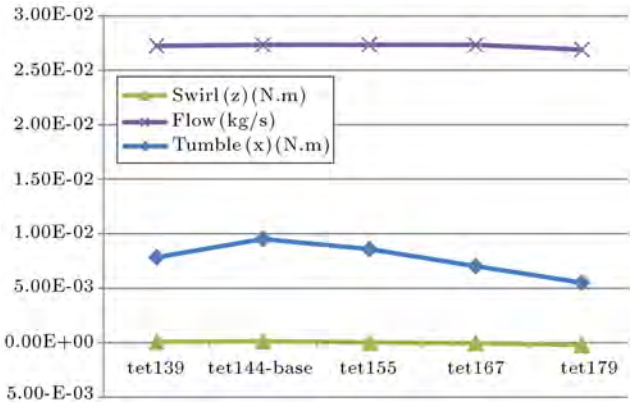

Figure 19. The effect of port angle on flow parameters.

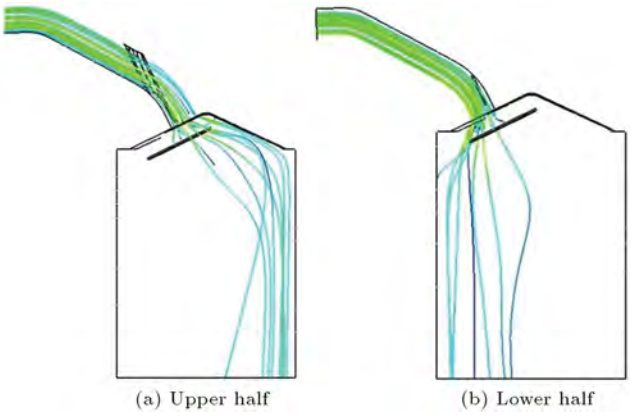

Figure 20. Half of port blocking.

flow characteristic of the intake port with θ equal to 144° is more preferable.

The results indicate that the variation of the port angle had virtually no effect on the swirl and the mass flow rate.

5. Intake port blockages

Another method of generating charge motion is to place flow blockages or vanes in the intake duct. In this section, the effects of flow blockage will be investigated.

5.1. Half of port blocking

One concept that can be used is blocking half the port section (Figure 20). The effects of these two patterns are shown in Figure 21.

It can be seen that the upper half of port blocking effectively reduces the flow over the short side of the intake port and directs more flow over the top of the intake valves. This leads to a stronger downward flow on the exhaust side of the chamber and, consequently, a stronger tumble motion is generated (about 25%) in the cylinder. The upper half of port blocking has good potential for a large tumble for applications in which we need a vortex to guide the fuel to the prescribed positions, e.g. to the spark plug, or the higher

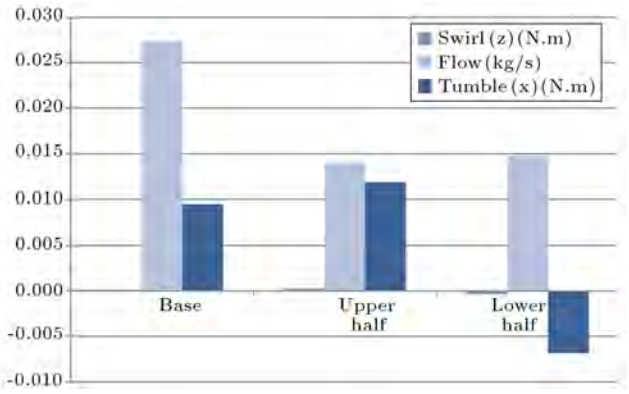

Figure 21. The effect of half of port blocking on flow parameters.

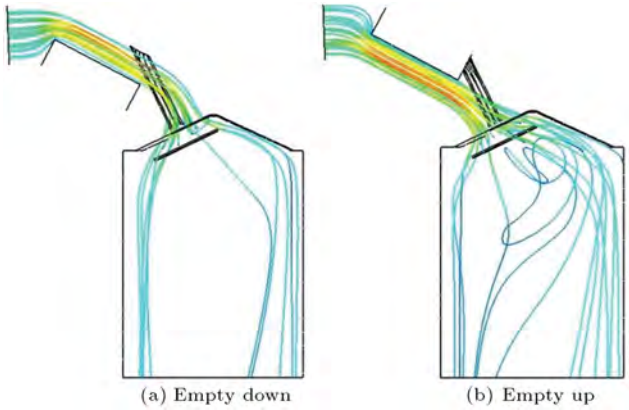

Figure 22. The effect of opening and closing half of port on flow parameters.

tumble motion is transformed into higher turbulence production. This translates into faster burn rates and fuel economy.

The lower half of port blocking directs flow to the intake side of the chamber and, consequently, the rotation tendency (sign of torque) will be reversed (Figures 20 and 21); a weaker tumble is generated (about 28%) in the reverse direction. In the lower half of port blocking, swirl intensity is produced noticeably. The last pattern will be useful for applications in which swirl flow is needed, e.g. for enhancing the fuel air mixing process. Also, as expected, port blocking reduces volumetric efficiency, the worst being the upper half of port blocking which delivers 48% lower flow rate.

5.2. Opening and closing half of port

Another concept that was studied is opening and closing half of the port section (Figure 22) and the effects of these patterns are shown in Figure 23. It can be seen that emptying the upper part of intake port effectively leads to a stronger tumble motion in the cylinder and swirl motion is produced noticeably. This pattern has good potential for a large tumble and swirl, simultaneously.

Emptying the lower part of the intake port has no

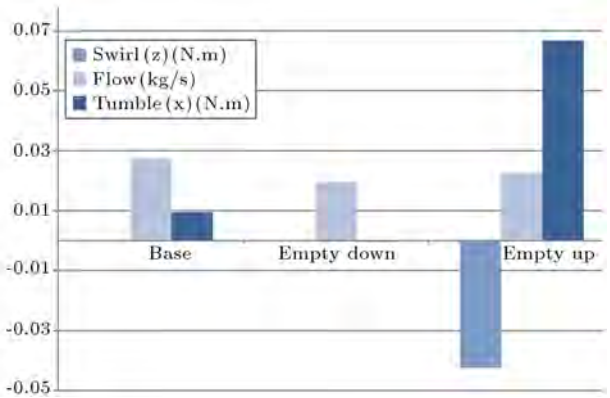

Figure 23. The effect of opening and closing half of port on flow parameters.

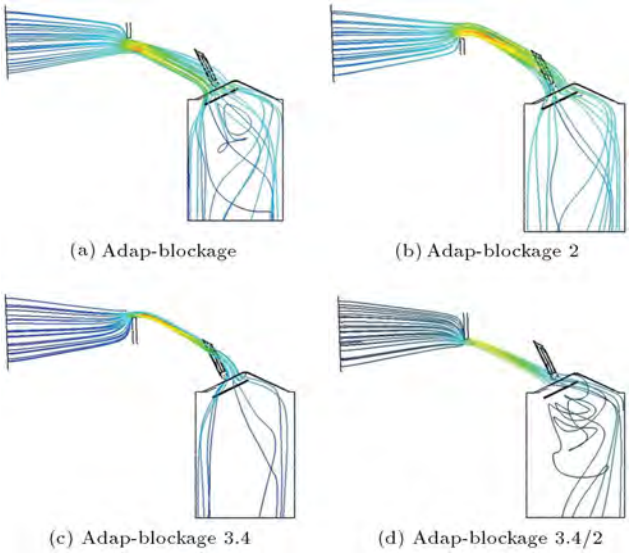

Figure 24. Step at intake port in four different patterns.

benefit to producing swirl or tumble and just reduces mass flow rate because of higher pressure loss. As expected, this concept decreases volumetric efficiency, which delivers 28% lower flow rate in the case of emptying the lower part, and 17% lower flow in the case of emptying the upper part.

5.3. Step at intake port

In this section, one plate is set at the intake port to block flow into the cylinder. Four patterns are simulated (Figure 24) as follows:

a) Blocking half of the section at the upper slice;

b) Blocking half of the section at the lower slice;

c) Blocking 3/4 of the section at the lower slice;

d) Blocking 3/4 of the section at the upper slice.

The effects of these patterns are shown in Figure 25. As shown, this step at the intake port has a negative effect on all parameters and cannot be useful.

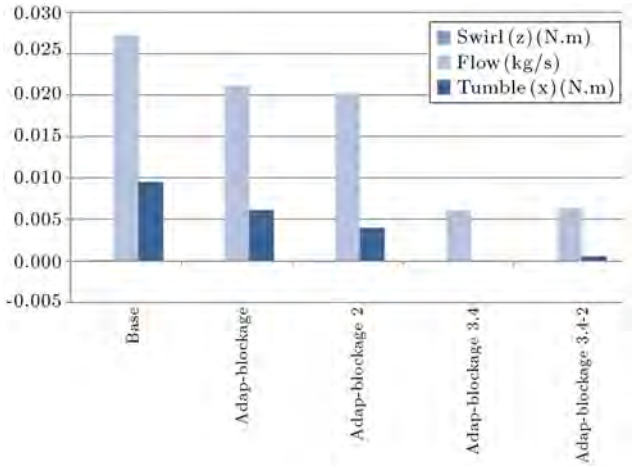

Figure 25. The effect of step at intake port on flow parameters.

6. Conclusion

The flowbench measurement adopted in this research is able to provide accurate quantitative answers. The simulation and experimental results are at reasonable levels of agreement. The discrepancy is acceptable to the engine designer.

The intake flow behavior was found to vary significantly as a function of valve lift. Specifically, it was found that at low lifts, the intake flow is relatively uniform around the periphery of the intake port, but, at high valve lifts, the flow into the cylinder is biased towards the top of the intake port. This results in a tendency to promote tumble at high valve lifts, but not at low valve lifts.

This paper provides a useful validation study for a range of turbulence models for in-cylinder flow. CFD analysis was employed to establish the relationship between design parameters and port flow characteristics. The CFD method can provide a digital reference for structure design and proves the feasibility of evaluation of the intake port by CFD application.

With the parametric study, new intake port design can be performed based on desirable flow parameters. Also, evaluation of the results shows that although these geometrical parameters have a considerable effect on tumble torque, their influence on swirl torque and mass flow rate seems negligible.

Finally, a numerical investigation into the various intake port blockage patterns, which are suitable options for controlling in-cylinder charge motion, is conducted. The proposed patterns allowed an increase in tumble or swirl generation for high load or for partial load requirements, respectively. Although all patterns had a negative impact on volumetric efficiency, they are useful for enhancing the turbulence of the charge at partial load, increasing the fuel burning rate and improving combustion efficiency.

Acknowledgment

The support given by the CAE Department of Irankhodro Powertrain Co. (IPCO) is greatly appreciated.

Nomenclature

MPI	Multi-Port Injection
BDC	Bottom Dead Center
TDC	Top Dead Center
CFD	Computational Fluid Dynamics
CAD	Computer Aided Design
RKE	Realizable $k-\varepsilon$ model
RNG	Renormalization group $k-\varepsilon$ model
RSM	Reynolds Stress linear Model
RSW	Reynolds stress omega model
SKE	Standard $k-\varepsilon$ model
SKW	Standard $k-\omega$ model
SST	Shear-stress transport $k-\omega$ model
A_{ref}	Reference area
B	Cylinder bore, swirl adapter fixture bore
C_d	Discharge coefficient
C_f	Flow coefficient
D_v	Inlet valve inner seat diameter
L_v	Valve lift
$\dot{m}_{\text{meas}}$	Measured mass flow rate
$\dot{m}_r$	Theoretical mass flow rate
p_0	Intake system pressure
p_T	Cylinder pressure
R	Gas constant
T_0	Intake system temperature
γ	Ratio of specific heat

References

1. Desantes, J.M., Galindo, J., Guardiola, J. and Dolz, C.V. "Air mass flow estimation in turbocharged diesel engines from in cylinder pressure measurement", *Experimental Thermal and Fluid Science*, **34**(1), pp. 37-47 (2010).
2. Blaxill, H. and Downing, J. "A parametric approach to spark-ignition engine inlet-port design", SAE 1999-01-0555 (1999).
3. Villiers, E. and Othmer, C. "Multi-objective adjoint optimization of intake port geometry", SAE 2012-01-0905 (2010).
4. Laget, O., Kleemann, A., Jay, S., Reveille, B. and Henriot, S. "Gasoline engine development using CFD", SAE Paper 2005-01-3814 (2005).

5. Toh, H., Huang, R.F., Lin, K.H. and Chern, M.J. "Computational study on the effect of inlet port configuration on in-cylinder flow of a motored four-valve internal combustion engine", *Journal of Energy Engineering*, **137**(4), pp. 198-206 (2011).
6. Huang, R.F., Lin, K.H. and Yeh, C.N. "In-cylinder tumble flows and performance of a motorcycle engine with circular and elliptic intake ports", *Exp. Fluids*, **46**, pp. 165-179 (2009).
7. Guy, R.K., Teipel, B.R. and Stanglmaier, R.H. "Use of computational fluid dynamics (CFD) tools for high-performance engine tuning", SAE Paper 2006-01-3666 (2006).
8. Le Coz, J.F., Henriot, S. and Pinchon, P. "An experimental and computational analysis of the flow field in a four-valve spark ignition engine-focus on cycle-resolved turbulence", SAE Paper 900056 (1990).
9. Son, J.W., Lee, S., Han, B. and Kim, W. "A correlation between re-defined design parameters and flow coefficient of SI engine intake ports", SAE 2004-01-0998 (2004).
10. Ramajo, D. and Nitro, N. "In-cylinder flow CFD analysis of a 4-valve spark ignition engine - Comparison between steady and dynamic tests", *J. Engine Gas Turbines and Power*, **132**(5), pp. 121-131(2010).
11. Ramajo, D. Zanotti, A. and Nigro, N. "In-cylinder flow control in a four-valve spark ignition engine: Numerical and experimental steady rig", *Proceedings of the Institution of Mechanical Engineers, Part D: Journal of Automobile Engineering*, **225**(6), pp. 813-828 (2011).
12. Selamet, A., Rupai, S. and He, Y. "An experimental study on the effect of intake primary runner blockages on combustion and emissions in SI engines under part-load conditions", SAE Paper 2004-01-2973 (2004).
13. Berntsson, A. Josefsson, G. Ekdahl, R. Ogink, R. and Grandin, B. "The effect of tumble flow on efficiency for a direct injected turbocharged downsized gasoline engine", SAE 2011-24-0054 (2011).
14. Gunasekaran, J. and Ganesan, V. "Effect of swirl and tumble on the stratified combustion of a DISI engine - A CFD study", SAE Paper 2011-01-1214 (2011).
15. Adomeit, P. "CAE-based port development and flow design for SI engines", SAE Paper 2005-01-0243 (2005).
16. Heim, D.M. and Ghandhi, J.B. "Investigation of swirl meter performance", *Proceedings of the Institution of Mechanical Engineers,Part D: Journal of Automobile Engineering*, **225**(8), pp. 1067-1077 (2011).

Appendix

The flow and discharge coefficient are defined as the ratio of the experimentally obtained mass flow rate, $\dot{m}_{\text{meas}}$, to the theoretical mass flow rate, $\dot{m}_r$:

$$C_f = \frac{\dot{m}_{\text{meas}}}{\dot{m}_r}. \tag{1}$$

If the flow is subsonic, the reference mass flow rate is given by:

$$\dot{m}_r = A_{\text{ref}}.\frac{p_0}{\sqrt{R.T_0}}.\left(\frac{p_T}{p_0}\right)^{1/\gamma}.\left\{\left[\frac{2.\gamma}{\gamma-1}\right].\left[1-\left(\frac{p_T}{p_0}\right)^{(\gamma-1)/\gamma}\right]\right\}^{1/2}, \tag{2}$$

while, if the flow is choked, the mass flow is calculated as follows:

$$\dot{m}_r = A_{\text{ref}}.\frac{p_0}{\sqrt{R.T_0}}.\gamma^{1/2}.\left(\frac{2}{\gamma+1}\right)^{(\gamma+1)/[2.(\gamma-1)]}. \tag{3}$$

When the intake phase is analyzed, p_0 is the intake system pressure, p_T is the cylinder pressure, T_0 is the intake system temperature and A_{ref} is the reference area.

The difference between the discharge and flow coefficient lies in the definition of the reference area, A_{ref} [10].

For the discharge coefficient, this area is the valve curtain area and, therefore, it is a linear function of valve lift, L_V :

$$A_{\text{ref}} = \pi.D_v.L_v. \tag{4}$$

For the flow coefficient, the reference area is given by the cylinder bore:

$$A_{\text{ref}} = \frac{\pi.B^2}{4}. \tag{5}$$

In order to compare the numerical and experimental results, the speed of each node was converted to the volume-average angular momentum:

$$T = \int_0^a abs(U)U_{\rho x}.dA, \tag{6}$$

where:

T	tumble torque (N.m);
U	velocity axial to the cylinder (m/s);
ρ	density (kg/m^3);
x	distance from axis of rotation (m);
a	area of the plane (m^2);
A	area (m^2).

The swirl torque was calculated, similarly.

Biographies

Abolfazl Mohammadebrahim received his BEng degree in Mechanical Engineering in 2005, and his MS degree in Automotive Engineering, in 2008, from the Iran University of Science and Technology (IUST).

He is currently a PhD student in the Department of Mechanical Engineering at Sharif University of Technology, Tehran, Iran. His research interests include internal combustion engine, fuels and combustion, and fluid mechanics.

Siamak Kazemzadeh Hannani received his PhD degree in Mechanical Engineering from the University of Lille, France, in 1996. He is currently member of the Center of Excellence in Energy Conversion and a Professor of Mechanical Engineering at Sharif University of Technology, Tehran, Iran. His research interests involve finite element, heat transfer, and turbulence modeling.

Behshad Shafii received his BEng degree in Mechanical Engineering from Sharif University of Technology, Tehran, Iran, in 1996, and his PhD degree in Mechanical Engineering from Michigan State University, USA, in 2005. He is currently Associate Professor in the Department of Mechanical Engineering at Sharif University of Technology, Tehran, Iran. His research interests include heat pipes, fluid diagnostic techniques (MTV, PIV, LIF), and heat transfer.